Accepted Manuscript

Carbon monoxide-releasing molecule-3 protects against cortical pyroptosis induced by hemorrhagic shock and resuscitation via mitochondrial regulation

Li-Min Zhang, Dong-Xue Zhang, Lan Fu, Yan Li, Xu-Peng Wang, Man-Man Qi, Chen-Chen Li, Pan-Pan Song, Xiao-Dong Wang, Xiang-Jun Kong

Please cite this article as: L.-M. Zhang, D.-X. Zhang, L. Fu, Y. Li, X.-P. Wang, M.-M. Qi, C.-C. Li, P.-P. Song, X.-D. Wang, X.-J. Kong, Carbon monoxide-releasing molecule-3 protects against cortical pyroptosis induced by hemorrhagic shock and resuscitation via mitochondrial regulation, *Free Radical Biology and Medicine* (2019), doi: https://doi.org/10.1016/j.freeradbiomed.2019.06.031.

Carbon monoxide-releasing molecule-3 protects against cortical pyroptosis induced by hemorrhagic shock and resuscitation via mitochondrial regulation

Li-Min Zhang[1, *], Dong-Xue Zhang[2], Lan Fu[3], Yan Li[1], Xu-Peng Wang[1], Man-Man Qi[1], Chen-Chen Li[1], Pan-Pan Song[1], Xiao-Dong Wang[1], Xiang-Jun Kong[4]

[1]Department of Anesthesiology, Cangzhou Central Hospital, Cangzhou, China

[2]Department of Gerontology, Cangzhou Central Hospital, Cangzhou, China

[3]Department of Radiodiagnosis, Cangzhou Central Hospital, Cangzhou, China

[4]Central Laboratory, Cangzhou Central Hospital, Cangzhou, China

* Corresponding author. Phone: +86 13343379856, E-mail addresses: azai2010@126.com

Conflict of interest statement

All authors certify that they have no affiliations with or involvement in any organization or entity with any financial interest, or non-financial competing interest in the subject matter or materials discussed in this manuscript by any of the authors.

Authors' contributions

Design of the study: Li-Min Zhang

Editing the manuscript: Li-Min Zhang, Yan Li

Statistical analysis: Li-Min Zhang, Dong-Xue Zhang

Experiment and data collection: Dong-Xue Zhang, Li-Min Zhang, Lan Fu, Yan Li, Xu-Peng Wang, Man-Man Qi, Chen-Chen Li, Pan-Pan Song, Xiao-Dong Wang, Xiang-Jun Kong

All authors read and approved the final manuscript.

Abstract

Objective: Carbon monoxide (CO) releasing molecule (CORM)-3, a water-soluble CORM, has protective effects against inflammatory and ischemia/reperfusion injury. We determined the effect of CORM-3 against neuronal pyroptosis in a model of hemorrhagic shock and resuscitation (HSR) in rats via mitochondrial regulation.

Methods: Rats were treated with CORM-3 (4 mg/kg) *in vitro* after HSR. We measured cortical CO content 3–24 h after HSR; assessed neuronal pyroptosis, mitochondrial morphology, ROS production, and mitochondrial membrane potential at 12 h after HSR; and evaluated brain magnetic resonance imaging at 24 h after HSR and learning ability 30 days after HSR. We also measured soluble guanylate-cyclase (sGC)-cyclic guanosine monophosphate (cGMP) signaling pathway activity using a blocker of sGC, NS2028, and ^{125}I-cGMP assay.

Results: Among rats that underwent HSR, CORM-3-treated rats had more CO in the cortical tissue than sham- and iCORM-3-treated rats. CORM-3-treated rats had significantly less neuronal pyroptosis in the cortical tissue; higher sGC activity and cGMP content; lower ROS production; better mitochondrial morphology, function, and membrane potential; and enhanced learning/memory ability than HSR-treated rats. However, these neuroprotective effects of CORM-3 were partially inhibited by NS2028.

Conclusion: CORM-3 may alleviate neuronal pyroptosis and improve neurological recovery in HSR through mitochondrial regulation mediated by the sGC–cGMP pathway. Thus, CO administration could be a promising therapeutic strategy for hemorrhagic shock.

Introduction

Severe hemorrhage among patients with trauma and those without trauma commonly induces incomplete brain perfusion and further causes neurological sequelae, most notably altered memory, mentation, seizures, and ischemic stroke[1, 2]. Although timely resuscitation is vital for treating hemorrhagic shock, systematic inflammatory response induced by this ischemia/reperfusion injury could cause further neuronal death, including pyroptosis[3, 4]. In recent years, pyroptosis has been shown to contribute to the development of ischemia/reperfusion injury[5, 6], and pyroptosis inhibition could improve long-term neurological function after cerebral ischemia/reperfusion injury[7].

A low of carbon monoxide (CO), which is an endogenous product of heme degradation by heme

oxygenase, confers increased resistance to inflammation triggered by lipopolysaccharide, ischemia/reperfusion injury, and other factors[8-10]. The application of CO-releasing molecule (CORM)-3 has emerged as an excellent alternative to CO administration[11]. Growing evidence has supported a role for mitochondrial regulation in CO-mediated neuroprotection against death and inflammation[12]. Recently, a study suggested that stimulation of the soluble guanylate-cyclase (sGC)-cyclic guanosine monophosphate (cGMP) signaling pathway attenuated ischemia/reperfusion-induced lung injury and suppressed ROS release[13]. Recent evidence also showed that improvement of mitochondrial dynamics can be protective against ischemia/hypoxia-induced elevation of ROS, mitoDNA, and calcium overload, which could further lead to pyroptosis[14, 15].

Whether CORM-3-mediated neuroprotective effects occur through the improvement of mitochondrial dynamics-induced pyroptosis is unclear. This study aimed to investigate whether CORM-3 attenuates hemorrhagic shock and resuscitation (HSR)-induced cerebral pyroptosis in a model of blood loss and re-infusion via mitochondrial regulation mediated by the sGC–cGMP pathway.

Key words: Carbon monoxide; neuroprotection; pyroptosis; soluble guanylate-cyclase; cyclic guanosine monophosphate

Abbreviations: CORM: Carbon monoxide releasing molecule; **sGC**: soluble guanylate-cyclase; **cGMP**: cyclic guanosine monophosphate; **ROS**: reactive oxygen species; **HSR**: hemorrhage shock and resuscitation; **MMP**: mitochondrial membrane potential

Results

Evoked potentials

Following three positive deflections generated from subcortical origin, a positive–negative–positive waveform (P8, N10.3, and P14.6) resembling the first primary cortical waves could be detected. N10.3 could be clearly detected in all animals and could easily be constantly affected by cortical ischemia. Thus, we opted to limit the investigation of potential to N10.3, as in a previous study[16] (Fig. 1A). There was a long-lasting difference between the Sham and HSR groups in somatosensory evoked potentials from 18.7 ± 3.5 min after HSR. The rats exposed to hemorrhagic shock exhibited a decrease of cortical function to approximately 30% of that at baseline at 15 min after bleeding and to 80% of that at baseline at 30 min after bleeding (vs. baseline, $P < 0.05$; Fig. 1B). These somatosensory evoked potentials were increased once resuscitation started (vs. 30 min after shock, $P < 0.05$; Fig. 1B) but did not reach baseline even if resuscitation ended (vs. baseline, $P < 0.05$; Fig. 1B).

HSR induced the peak of neuronal pyroptosis 12 h after resuscitation

At 6, 12, and 24 h after HSR, results of immunofluorescence assays revealed that neuronal pyroptosis in the cortical tissue was significantly increased after HSR compared with that in the Sham group (vs. Sham, $P < 0.05$; Fig. 2B). Compared with 6 h after HSR, increases in neuronal pyroptosis were markedly shown at 12 h (vs. 6 h after HSR, $P < 0.05$; Fig. 2B). However, a decrease was revealed at 24 h after HSR compared with that at 12 h (vs. 12 h after HSR, $P < 0.05$; Fig. 2B).

CORM-3 inhibited neuronal pyroptosis after HSR via CO upregulation

When a blood loss and re-infusion model was established in rats, a water-soluble exogenous CO donor, CORM-3, was applied to rats after resuscitation via a single intravenous injection; inactive CORM-3 (iCORM-3), which does not release CO, was used as a negative control. CO content was increased within 6 h after HSR compared with that in the Sham group (vs. Sham, $P < 0.05$; Fig. 3B). Figure 2B also shows that CO content in the HSR/CORM-3 group declined after 6 h (vs. HSR, $P < 0.05$; Fig. 3B). CORM-3 administration could further elevate the total cortical CO level 3–24 h after HSR compared with that after HSR alone and after HSR/iCORM-3 (vs. HSR, $P < 0.05$; vs. HSR/iCORM-3, $P < 0.05$; Fig. 3B). CORM-3 treatment induced the peak of CO concentration at 6 h

after HSR exposure (vs. 3h, 12 h and 24 h after HSR/CORM-3, $P < 0.05$; Fig. 3B). In addition, there were no significant differences between the HSR and HSR/iCORM-3 groups.

Immunofluorescence double staining of cleaved caspase-1 and neuronal nuclei (NeuN) showed that iCORM-3 co-administration at 12 h after HSR in the HSR/iCORM-3/Vehicle group failed to reduce the number of cleaved caspase-1-positive neurons in the cortical tissue (vs. Sham/iCORM-3/Vehicle, $P < 0.05$; Fig. 4B), whereas CORM-3 reduced pyroptosis after HSR alone in the HSR/CORM-3/Vehicle group (vs. HSR/iCORM-3/Vehicle, $P < 0.05$; Fig. 4B). Compared with the Sham/iCORM-3/Vehicle group, neuronal pyroptosis remained elevated in the HSR/CORM-3/Vehicle group (vs. Sham/iCORM-3/Vehicle, $P < 0.05$; Fig. 4B). Pyroptosis depends on caspase-1 activation, leading to IL-1β and IL-18 stimulation, cytomembrane pore formation, and subsequently the release of inflammatory mediators and cellular contents[17]. IL-1β and IL-18 expression was also measured at 12 h after HSR. HSR exposure plus iCORM-3 co-administration caused significant increases in IL-1β and IL-18 expression compared with that in the Sham/iCORM-3/Vehicle group (vs. Sham/iCORM-3/Vehicle, $P < 0.05$; Fig. 4D, 4E). Compared with HSR/CORM-3/Vehicle, CORM-3 co-administration after HSR downregulated IL-1β and IL-18 expression in the cortical tissue (vs. HSR/CORM-3/Vehicle, $P < 0.05$; Fig. 4D, 4E).

NS2028 inhibited the protective effect of CORM-3

sGC enzyme activity and cGMP content were further examined. As shown in Figure 4F, at 12 h after HSR plus iCORM-3 treatment, the basal sGC enzyme activity in the cortical tissue was significantly lower after HSR than in the Sham group (vs. Sham/iCORM-3/Vehicle, $P < 0.05$; Figure 4F). Consistent with decreased sGC activity after HSR plus iCORM-3 treatment, cGMP content in the cortical tissue of rats was significantly decreased after HSR compared with that in the Sham group (vs. Sham/iCORM-3/Vehicle, $P < 0.05$; Figure 4G). CORM-3 partially restored the sGC activity and cGMP content in rats exposed to HSR (vs. HSR/iCORM-3/Vehicle, $P < 0.05$; Figure 4F, 4G).

To explore the potential role of sGC in CORM-3's effect against pyroptosis, NS2028, an inhibitor of sGC, was applied to rats before bleeding. NS2028 pre-treatment induced the decreases in the sGC enzyme activity and cGMP content in Sham/iCORM-3/NS2028 (vs. Sham/iCORM-3/Vehicle, $P < 0.05$; Fig. 4F, 4G) and in Sham/CORM-3/NS2028 (vs. Sham/CORM-3/Vehicle, $P < 0.05$; Fig. 4F, 4G). Moreover, NS2028 pre-treatment inhibited the decreases in neuronal pyroptosis and IL-1β/IL-18

expression as well as the increases in the sGC enzyme activity and cGMP content when rats were exposed to HSR+CORM-3 (vs. HSR/CORM-3/Vehicle, P < 0.05; Fig. 4B, 4D–G). There was no significant difference of neuronal pyroptosis and IL-1β/IL-18 expression between the Sham/iCORM-3/NS2028 and Sham/iCORM-3/Vehicle groups, as well as Sham/CORM-3/NS2028 and Sham/CORM-3/Vehicle groups. Neuronal pyroptosis and IL-1β and IL-18 expression were further increased in the model of NS2028 pre-treatment before HSR plus iCORM-3 compared with those for HSR alone (vs. HSR/iCORM-3/Vehicle; P < 0.05; Fig. 4B, 4D, 4E). Moreover, the sGC enzyme activity and cGMP content were significant lower after HSR/iCORM-3/NS2028 treatment than after HSR alone (vs. HSR/iCORM-3/Vehicle; P < 0.05; Fig. 4F, 4G).

CORM-3 treatment improved mitochondrial injury after HSR

To determine the morphology of mitochondria from the cortical tissue, at 12 h after HSR, an electron microscopic study was performed. Results revealed that iCORM-3 did not prevent dysmorphic mitochondria characterized by (a) degenerative changes, for example, matrix vacuolation, disarrangement of cristae, swelling, and partial cristolysis and (b) necrosis, characterized by complete cristolysis or ghost cells. The prevalence of dysmorphic mitochondria, as well as swelling plus ghost mitochondria, in the cortical tissue of HSR/CORM-3/Vehicle-treated rats was significantly lower than that in HSR/iCORM-3/Vehicle-treated rats (vs. HSR/iCORM-3/Vehicle; P < 0.05; Fig. 5B, 5C). However, NS2028 pre-treatment before HSR plus CORM-3 treatment upregulated the prevalence of dysmorphic mitochondria and swelling plus ghost mitochondria compared with that after HSR plus CORM-3 treatment (vs. HSR/CORM-3/Vehicle; P < 0.05; Fig. 5B, 5C). In addition, NS2028 further worsened mitochondrial morphology in HSR/iCORM-3/NS2028-treated rats compared with that in HSR/iCORM-3/Vehicle-treated rats (vs. HSR/iCORM-3/Vehicle; P < 0.05; Fig. 5B, 5C). There was no significant difference in mitochondrial morphology between the Sham/iCORM-3/NS2028 and Sham/iCORM-3/Vehicle groups, as well as Sham/CORM-3/NS2028 and Sham/CORM-3/Vehicle groups.

Mitochondrial membrane potential, indicated by JC-1 fluorescence, was used to reveal mitochondrial depolarization after hemorrhagic shock. ROS-mediated mitochondrial damage after reperfusion could release damage-associated molecular pattern molecules, which can initiate the

progress of pyroptosis. At 12 h after HSR plus iCORM-3 treatment, those exposure caused a significant decrease in the mitochondrial membrane potential of the cortical tissue as well as an increase in mitochondrial ROS compared with those in the Sham plus iCORM-3 group (HSR/iCORM-3/Vehicle vs. Sham/iCORM-3/Vehicle, $P < 0.05$; Fig. 5D, 5E). In HSR/CORM-3/Vehicle group, CORM-3 administration after HSR upregulated mitochondrial membrane potential and downregulated mitochondrial ROS production (vs. HSR/iCORM-3/Vehicle, $P < 0.05$; Fig. 5D, 5E), whereas NS2028 pre-treatment before HSR partially inhibited these improvements in mitochondrial membrane potential and ROS (vs. HSR/CORM-3/Vehicle; $P < 0.05$; Fig. 5D, 5E). NS2028 pre-treatment before HSR also further worsened mitochondrial membrane potential and mitochondrial ROS production in the HSR/iCORM-3/NS2028 group compared with those in the HSR/iCORM-3/Vehicle group (vs. HSR/iCORM-3/Vehicle, $P < 0.05$; Fig. 5D, 5E). There were no marked changes between the Sham/iCORM-3/NS2028 and Sham/iCORM-3/Vehicle groups, as well as Sham/CORM-3/NS2028 and Sham/CORM-3/Vehicle groups.

CORM-3 treatment after HSR improved cortical changes revealed by T2-weighted MRI

T2-weighted images revealed there was no significant differences between the sham groups (Fig. 6B). At 24 h after HSR, a significant increase of the ratio of standardized signal intensity (SSI) before/after shock on regions of cerebral cortex was shown in the HSR groups compared with their sham counterparts (Fig. 6B). In HSR/CORM-3/Vehicle group, CORM-3 administration after HSR downregulated the hyperintensity lesions indicated by ratio of SSI (vs. HSR/iCORM-3/Vehicle, $P < 0.05$; Fig. 6B), whereas NS2028 pre-treatment before HSR partially inhibit these improvements in hyperintensity lesions (vs. HSR/CORM-3/Vehicle; $P < 0.05$; Fig. 6B). NS2028 pre-treatment before HSR also further increased the ratio of SSI in the HSR/iCORM-3/NS2028 group compared with those in the HSR/iCORM-3/Vehicle group (vs. HSR/iCORM-3/Vehicle, $P < 0.05$; Fig. 6B). There were no significant changes between the Sham/iCORM-3/NS2028 and Sham/iCORM-3/Vehicle groups, as well as Sham/CORM-3/NS2028 and Sham/CORM-3/Vehicle groups.

CORM-3 treatment after HSR improved learning ability

We examined whether learning ability was involved in incomplete ischemia/reperfusion induced by hemorrhagic shock. When tested 30 days after exposure, HSR plus iCORM-3-treated rats located the

submerged platform with significantly slower latencies than Sham plus iCORM-3-treated rats (vs. Sham/iCORM-3/Vehicle, $P < 0.05$; Fig. 7C–E). There was no difference in latency between the Sham/iCORM-3/Vehicle and Sham/CORM-3/Vehicle groups. CORM-3 administration after HSR resulted in a significantly faster latency to locate the submerged platform than that of HSR plus iCORM-3-treated rats (HSR/CORM-3/Vehicle vs. HSR/iCORM-3/Vehicle, $P < 0.05$; Fig. 7C–E). A slower latency to locate the submerged platform was noted in HSR/CORM-3/NS2028-treated rats than that in HSR/CORM-3/Vehicle-treated rats (vs. HSR/CORM-3/Vehicle, $P < 0.05$; Fig. 7C–E). There was no difference in latency between the HSR/iCORM-3/NS2028 and HSR/CORM-3/NS2028 groups.

The time and distance spent in the targeted quadrant in rats exposed to HSR plus iCORM-3 exposure were severely reduced compared with those in the Sham/iCORM-3/Vehicle group (vs. Sham/iCORM-3/Vehicle, $P < 0.05$; Fig. 7F, 7G). Figure 7 also reveals that HSR/CORM-3/Vehicle treatment markedly increased the time and distance compared with HSR/iCORM-3/Vehicle (vs. HSR/iCORM-3/Vehicle, $P < 0.05$; Fig. 7F, 7G). NS2028 pre-treatment before HSR inhibited the improvement of CORM-3 against HSR-induced decreases of time and distance (vs. HSR/CORM-3/Vehicle, $P < 0.05$; Fig. 7F, 7G). In addition, NS2028 pre-treatment before HSR in the HSR/iCORM-3/NS2028 group further downregulated the time and distance in the targeted quadrant compared with those in the HSR/iCORM-3/Vehicle group (vs. HSR/iCORM-3/Vehicle, $P < 0.05$; Fig. 7F, 7G). Additionally, there were no prominent differences of time and distance between the Sham/iCORM-3/NS2028 and Sham/iCORM-3/Vehicle groups, as well as Sham/CORM-3/NS2028 and Sham/CORM-3/Vehicle groups.

Discussion

In the present study, HSR using a model of blood loss and re-infusion decreased somatosensory evoked potentials; caused degeneration of learning ability and attenuation of the sGC activity and cGMP content; increased cortical injury (indicated by pyroptosis), T2-weighted MRI, and ROS level; and induced ultrastructural changes in the mitochondria. CORM-3 administration after resuscitation provided neuroprotection for HSR, whereas this neuroprotective effect could be inhibited by a blocker of sGC (NS2028).

Long-term hypotension and hypovolemia induced by hemorrhagic shock lead to hypoperfusion,

subsequently resulting in incomplete ischemic injury[18]. In our previous study, we reported that incomplete cerebral ischemia/reperfusion in a model of HSR-induced severe neuronal injury in the hippocampus[19]. Here, the obtained results reveal that HSR not only significantly decreased somatosensory evoked potentials sensitive to cortical hypoxia but also increased cortical hyperintensity, as indicated by T2-weighted MRI, which supported the findings of previous studies[20]. Increasing evidence suggests that ischemia causes neuronal damage in the cortical tissue and leads to learning ability impairments[21, 22]. Decreased learning ability was associated with a reduction of perfusion induced by hemorrhagic shock.

The major pathogenic mechanisms of cerebral ischemia/reperfusion injury include excitotoxicity, peri-infarct depolarizations at the early stage, inflammation at the middle stage, and programmed cell death at the end stage[23]. Incomplete cerebral ischemia/reperfusion induces significant neuronal injury, including necrosis and apoptosis[24, 25]. Pyroptosis, unlike apoptosis or necrosis, is a novel form of programmed cell death. The initiation of pyroptosis depends on caspase enzyme-1 (caspase-1) and is accompanied by the release of large amounts of IL-1β and IL-18. There is increasing evidence that post-ischemic inflammation, involving IL-1β and IL-18, contributes to ischemic brain injury[23]. Cellular edema, which presents as high-signal lesions on T2-weighted imaging, involves oncotic swelling of the neuronal cells due to a shift of ions (mainly Na^+) and water molecules from a pore in the plasma membrane to intracellular as a consequence of ischemic energy depletion. IL-1β and IL-18 play vital roles in forming this pore. The expression of cleaved caspase-1 combined with IL-1β and IL-18 is generally used to assess the pyroptosis level. Shu et al. reported that transient global cerebral ischemic/reperfusion in vivo and oxygen/glucose deprivation in vitro induce neuronal pyroptosis mediated by the caspase-1/IL-18, IL-1β pathway[24, 26]. The present study revealed increased neuronal pyroptosis in a model of blood loss and re-infusion, and cortical hyperintensity was also increased, as revealed by T2-weighted imaging. Moreover, our study also demonstrated that at 12 h after HSR, neuronal pyroptosis peaks, characterized by caspase-1 activation and release of inflammatory factors, which is in accordance with inflammatory death in the middle stage after ischemia[23].

CORM-3 suppressed inflammasome signaling and the occurrence of pyroptosis, which consequently alleviated neuronal death and improved motor functional recovery following spinal cord injury[27]. In the current study, it was revealed that CORM-3 treatment induced the peak of CO concentration at 6 h

after HSR exposure. Although there was not a significant peak at 6 h in the HSR and HSR+iCORM-3 group, a growing trend within after HSR could be found. Inoue et.al reported that hemorrhage shock induced a peak of heme oxygenase-1 (HO-1) at 6 h after resuscitation[28]. It might be associated with the increases of CO generated from heme via HO-1[29]. CORM-3 reduced neuronal pyroptosis and production of relevant inflammatory factors, including IL-18 and IL-1β. Interestingly, CORM-3 partially restored the sGC activity and cGMP content in rats exposed to HSR. To further confirm the exact mechanism involved, NS2028, an sGC inhibitor, was administered via femoral vein injection after resuscitation. Our results revealed that NS2028 partially inhibited the neuroprotection of CORM-3 against HSR injury. sGC activation and increases in the cGMP content via CO would be responsible for decreases in ROS production and improvement of mitochondrial integrity[12]. CORM-3 after resuscitation decreased ROS production, which may be dependent on the sGC–cGMP signaling pathway. Decreased mPTP opening and increased mitoKATP opening could be induced via the activation of the sGC–cGMP signaling pathway[30, 31]. Misawa et al. also reported that the spatial arrangement of the mitochondria may promote the activation of caspase-1-associated pyroptosis[32]. The pyroptosis may also respond to mitochondrial stress, such as ROS[33]. CO controls mitochondrial integrity via the regulation of mitochondrial biogenesis and mitophagy[34]. Therefore, the protective effect of CO against mitochondrial stress might provide a potential interpretation of pyroptosis signaling by CORM-3.

The limitations of this study include the fact that the study was focused on effects of HSR alone. The models of HSR with tissue injury, such as traumatic brain injury plus HSR, should be further studied. Moreover, present data only showed that sGC plays a vital role in CO-induced neuroprotection, but whether CO improves these injuries induced by HSR via sGC–cGMP–PKG or other signaling pathways, such as nNOS[35], remains unclear. In addition, the present study did not focus on whether pyroptosis depended on the GSDMD and caspase-11 signaling pathways[36]. Further studies on models and feasible signaling pathways should be performed.

In conclusion, this study showed that neuroprotective effects of CORM-3 against neuronal pyroptosis after HSR injury might be associated with the sGC–cGMP signaling pathway.

Methods

All animal experiments were performed in accordance with the National Institutes of Health Guidelines

for the Care and Use of Laboratory Animals. Formal approval to conduct the experiments was obtained from the Animal Review Board of Cangzhou Central Hospital.

Group assignment

Rats were randomly assigned (computer-based randomization) to one of the following eight groups: (1) Sham/iCORM-3/Vehicle group, catheters to the left femoral artery and vein were inserted using an indwelling needle (22 G) as surgical preparation, 76 min later, iCORM-3 (4 mg/kg, intravenous, S744801; Selleck, USA) was injected accordance with our prior experiments and previous study[37]; (2) Sham/iCORM-3/NS2028 group, rats were treated with surgical preparation, NS2028 (10 mg/kg, intravenous) was injected accordance with our prior experiments, and 75 min later, iCORM-3 (4 mg/kg, intravenous) was injected; (3) Sham/CORM-3/Vehicle group, rats were treated with surgical preparation, and 76 min later, CORM-3 (4 mg/kg, intravenous, S744801; Selleck, USA) was injected; (4) Sham/CORM-3/NS2028 group, rats were treated with surgical preparation, NS2028 (10 mg/kg, intravenous) was injected, and 75 min later, CORM-3 (4 mg/kg, intravenous) was injected; (5) HSR/iCORM-3/Vehicle group, rats were treated with surgical preparation, hemorrhagic shock was induced by blood loss for 45 min, resuscitation was performed with blood re-infusion for 15 min, and iCORM-3 (4 mg/kg, intravenous) was then injected; (6) HSR/iCORM-3/NS2028 group, rats were treated with surgical preparation, NS2028 (10 mg/kg, intravenous) was injected before HSR, iCORM-3 (4 mg/kg, intravenous) was then injected after resuscitation; (7) HSR/CORM-3/Vehicle group, rats were treated with surgical preparation, CORM-3 (4 mg/kg, intravenous) was then injected after HSR; (8) HSR/CORM-3/NS2028 group, rats were treated with surgical preparation, NS2028 (10 mg/kg, intravenous) was injected before HSR, CORM-3 (4 mg/kg, intravenous) was then injected after resuscitation. The inactive compound iCORM-3 was prepared by dissolving CORM-3 in PBS and incubating for 24 h under air and light exposure. After 24 h, the solution was bubbled with nitrogen to remove residual CO. NS2028 was prepared as described above immediately before use.

HSR protocol

Sprague–Dawley male rats weighing 350–400 g were used to establish the HSR model. Rats were housed in individual shoebox cages with bedding. The room temperature was maintained at 25°C ± 1°C with alternating 12-h light/12-h dark cycles. Rats were allowed free access to water and a chow

diet until the start of the experiments. As in our previous study[19], rats were cannulated with a heparinized polyethylene tube via the left femoral artery for blood pressure measurement and via the left femoral vein for hemorrhage shock induction after anesthesia with sevoflurane (7%–8% for induction, and 3%–4% for maintenance). After tracheal intubation, rats were mechanically ventilated via a volume-controlled ventilator (ALC-V; Shanghai Alcott Biological Technology Inc., Shanghai, China) with a tidal volume of 4 ml/100 g, initial respiratory frequency of 70 bpm, and FiO_2 of 40%. Respiratory frequency was adjusted to an end-tidal carbon dioxide [$ETCO_2$] (PMSH-300; SunLife Science Inc., Shanghai, China) pressure between 35 and 40 mmHg. Hemorrhagic shock was initiated by bleeding into a heparinized syringe (10 U/mL) to maintain a mean arterial pressure of 30 ± 5 mmHg for 60 min. Resuscitation was performed by returning all shed blood and, if necessary, administering sterile saline to the baseline level. Body temperature was maintained within 35°C–38°C by an electric heating pad.

Evoked potentials

The median nerves were percutaneously stimulated (DS2; Digitimer, Welwyn Garden City, UK) at the ankle (10 Hz, twice supramaximally), with recording electrodes on the skull (−2 mm from the bregma, 2.5 mm from the midline) and reference electrodes on the nearby inactive tissue. The ground electrode was inserted under the lumbar skin. Potentials were stimulated by a Dantec Type 15E07 constant current stimulator and recorded with a Dantec 15C01 EMG amplifier. Amplified waveforms were further analyzed by Dasy Lab 3.00 (Datalog GmbH, Mönchengladbach, Germany).

Carbon monoxide content detection

The CO content in the cortical tissue was detected using an endogenous carbon monoxide assay kit (Nanjing Jiancheng Bioengineering Institute, Nanjing, China), as previously described (n = 6 per group)[27]. Specific steps were conducted in accordance with the manufacturer's instructions. Briefly, cortical tissue samples were removed at 3, 6, 12, and 24 h after HSR. After homogenizing in PBS, the sample (0.5 mL) was added into Hb solution (1 mL). Following vortexing and quiescence, mixtures were measured at 541 nm (as absorbance) and 555 nm (as a reference). Ratio of the 541-nm- to 555-nm readings was recorded and used to calculate the CO content of samples.

sGC activity assay

For quantitative sGC activity assays, a mixture including 200 mg of cortical tissue and 1.8 mL of enzyme extract buffer [5 mM Tris-HCl (pH 8.0), 1 mM EDTA, 2 mM phenylmethylsulfonyl fluoride, and 0.25 mM sucrose] was homogenized (n = 6 per group). Following centrifugation for 10 min (1,000×g, 4°C), the supernatant was further centrifuged for 1 h (105,000×g, 4°C), and protein content of the supernatant was measured using a BCA protein assay (Beyotime, Wuhan, China). Ten microliters of sample was incubated with 90 μL of reaction buffer [50 mM Tris-HCl (pH 7.5), 4 mM $MnCl_2$, 0.5 mM 3-isobutyl-1-methyxanthine (IBMX), 15 mM creatine phosphate, 240 U/L creatine phosphokinase, 1 mM GTP, and 1 mM sodium nitroprusside]. After terminating the reaction with 0.2 mM sodium acetic acid, cGMP production was detected using a ^{125}I-cGMP kit (Shanghai Ruiqi Biotech, Shanghai, China), in accordance with the manufacturer's instructions. The sGC enzyme activity was expressed as picomoles of cGMP synthesized per min per mg of cortical tissue protein (pmol cGMP/mg protein/min).

Measurement of the basal cGMP content

Fifty milligrams of the cortical tissue mixed with 1 mL of buffer containing 50 mM sodium acetic acid, 4 mM EDTA, and 10 mM 3-isobutyl-1-methyxanthine at 4°C was extracted with dehydrated ethanol (n = 6 per group). After centrifuging for 15 min at 3,500×g, the supernatant was taken and dried at 60°C, and cGMP production was detected using a ^{125}I-cGMP kit as described above.

Mitochondrial extraction and electron microscopy studies

At 6 h after HSR, mitochondria from the cortical tissues were extracted as per a previous study (n = 6 per group)[38]. Briefly, homogenates of the hippocampal tissues were centrifuged twice at 1,000×g and 4°C for 5 min, and supernatant was then centrifuged at 15,000×g and 4°C for 2 min. The supernatant was removed with careful elimination of all fat and fluffy layers on the top of the pellet containing mitochondria. To eliminate harmful enzymes, nucleases, phospholipases, and proteases, pellets from two tubes were combined, resuspended in 1.5 mL of ice-cold buffer, and centrifuged at 15,000×g and 4°C for 2 min. The final pellet was resuspended in ice-cold final equilibrated buffer (250 mM sucrose, 5 mM KH_2PO_4, 10 mM Tris-HCl, 2 mg/mL BSA, pH 7.2). These pellets were fixed in 2.5% glutaraldehyde in 0.1 M sucrose phosphate buffer (SPB) for 1 h. After washing with 0.1 M SPB,

mitochondrial extractions were fixed with 1% osmium tetroxide in 0.1 M SPB for 1 h. Following washing with 0.1 M SPB, pellets were dehydrated in graded ethanol, infiltrated with LR white resin (Sigma-Aldrich, Poole, UK), embedded in capsule beams, and finally polymerized at 65°C for 48 h. After cutting into serial ultrathin slices (50 nm) with an ultramicrotome, slices were stained with 4% uranyl acetate-lead citrate, and the ultrastructure of the mitochondrial pellets was observed under a transmission electron microscope (JEM-2000EX; JEOL, Tokyo, Japan). Dysmorphic mitochondria were examined, counted, and calculated in terms of percentage/field at 3000× magnification, including swelling plus ghost as well as normal mitochondria, as mentioned in a previous study[39].

Assessment of mitochondrial ROS

For the quantitative measurement of intracellular ROS, the fluorometric method was used (n = 6 per group). In brief, at 12 h after HSR, the cortical tissues (1 mg/0.1 ml) were mixed with ROS assay medium (2.9 mL) in one reaction system, and in the other reaction system, 3 μL of 5 mmol/L 2′,7′-dichlorofluorescin diacetate (DCFH-DA) was added to 3.3 mmol/L succinic acid as a substrate without mitochondria. The above two reaction systems were incubated at 37°C for 15 min. The fluorescence intensity of the substrate without mitochondria (F1) and that of the sample with cortical tissues (F) were measured. The ROS production rate was calculated by subtracting F1 from F[40].

Mitochondrial membrane potential assay

For quantitative measurement of mitochondrial membrane potential (MMP), JC-1, a mitochondrion-selective dye, was used to determine each sample from the above seven groups, as in our previous study (n = 6 per group)[19]. At 12 h after HSR, the mitochondria isolated from the cortical tissues were stained with JC-1 (5 μg/ml; Beyotime Institute of Biotechnology, Beijing, China) for 30 min at 37°C in the dark. After rinsing twice with assay buffer, fluorescent intensity was analyzed on a spectrofluorometer (Paradigm; Molecular Devices, Sunnyvale, CA, USA), as described previously, to detect green fluorescence at excitation/emission wavelengths of 485/530 nm and red fluorescence at excitation/emission wavelengths of 550/595 nm. The ratio of red/green fluorescence intensity was determined for each sample as a measure of MMP.

Cleaved caspase-1/NeuN/DAPI immunofluorescence

Cortical tissues were fixed in 10% neutral-buffered formalin under anesthesia with sevoflurane, embedded in paraffin, and sectioned at 10-μm thickness (n = 6 per group). Immunofluorescence staining was performed to determine the percentage of neuronal pyroptosis. Briefly, paraffin sections were dewaxed and hydrated for 10 min at room temperature and then incubated with the primary polyclonal rabbit antibody against cleaved caspase-1 (1:500, ab1872; Abcam, UK) and polyclonal mouse against NeuN antibody (1:500, ab104224; Abcam, UK) overnight at 4°C. Sections were then washed again thrice in PBS before incubation in the dark for 1 h in blocking solution containing the secondary antibodies (CyTM3-conjugated goat anti-rabbit IgG, 1.5 mg/mL, A0516, Beyotime, China; FITC-conjugated goat anti-mouse IgG, 1.5 mg/mL, A5608, Beyotime, China) diluted at 1:200 in the blocking solution. After washing with PBS, 5 μg/mL 2-(4-amidinophenyl)-6-indolecarbamidine dihydrochloride (DAPI; Beyotime Biotech Inc., Nantong, China) was added to stain the cell nuclei for 2 min to show their locations. Immunofluorescence images were captured using a laser scanning confocal microscope (Olympus, Tokyo, Japan), and the percentage of cleaved caspase-1 combined with NeuN- and DAPI-positive cells was calculated.

Western blotting

IL-1β and IL-18 expression levels were assessed using Western blotting (n = 6 per group). At 12 h after HSR, total protein was extracted from the cortical tissues and lysed in tissue lysis buffer. Samples containing 30 μg of protein were subjected to SDS-PAGE and transferred onto a membrane. After the membrane had been blocked at 37°C for 2 h, primary antibodies of rabbit anti-rat polyclonal IL-1β (1:1000 dilution, ab9722; Abcam, USA) and IL-18 (1:1000 dilution, ab71495; Abcam, USA) antibody were applied at 4°C overnight, followed by incubation with a secondary antibody (anti-rabbit antibody, 1:2000 dilution, sc-2004; Santa Cruz Biotechnology, Inc., Santa Cruz, CA, USA) at 25°C for 1 h. Protein bands in each treatment group were detected using a Western blot detection system with ECL (Amersham Biosciences, Piscataway, NJ, USA). β-Actin (1:2000 dilution, sc-47778; Santa Cruz Biotechnology, Inc.) was used as an internal reference[41].

MRI study

MRI was performed using a clinical 2.0 T MRI scanner (Magnetom, version 2.0 T; Siemens, Berlin, Germany) along with a general 3-in circular coil at room temperature. T2-weighted images were

acquired using the following parameters: repetition time (TR)/echo time (TE), 2500/70; 6 echoes, 192 × 192; slices, 12; slice thickness, 2.0 mm; field of view (FOV), 80 mm; and acquisition time, 6.5 min. For all models at 24 h after HSR, rats were then placed prone in an animal holder, and the four-element proton surface coil array was positioned and fixed over the head of the animal after applying anesthesia with sodium pentobarbital as described above. ImageJ analysis and processing was applied for T2W images. Besides visual inspection, the regions of interest (ROI) were placed free-hand on regions of cerebral cortex, and signal intensity before and after indicated stimuli were measured. To reflect the signal changes on T2WI, T2-weighted standardized signal intensity (SSI) was obtained by calculating the ratios between the average signal intensity (SI) and SI of temporalis. The ratio of before/after indicated stimuli SSI was determined for each rat as a measure of T2W images.

Morris water maze test

Thirty days after HSR, a Morris water maze was used to assess the learning ability following the indicated stimuli (n = 6 per group). Behavioral tests were assessed by an investigator blinded to the experimental groups. A black-painted circular pool (diameter, 100 cm; depth, 30 cm) was filled with warm water (25 ± 1°C) to a depth of 25 cm. A transparent platform (diameter, 10 cm; height, 29.5 cm) was placed in a constant location during the acquisition phase. The experimental room contained distinctive distal visual cues surrounding the pool that remained unchanged throughout the study. A video-tracking system (Shanghai Mobiledatum Co., Ltd., Shanghai, China) was used to record the movement (from latency to the platform). Before the training session, rats were kept on the platform for 30 s and were given 90 s to find the platform when they were placed in water from one of four starting quadrants (in a random order). The training test took place four times a day for 4 days. Thirty-four days after HSR, the distance and time spent in the targeted quadrant were recorded[42].

Statistics

All statistical analyses were conducted using SPSS 17.0 for Windows (SPSS, Inc., Chicago, IL, USA). Data are given as mean ± standard deviation (SD). The assumption of homogeneity of variance was checked using the Levene test. When data heteroscedasticity was identified, it was corrected by logarithmic transformation of the data. Data were compared using multi-factor analysis of variance (ANOVA) with a Tukey post hoc test. Differences with $P < 0.05$ were considered significant.

References

[1] P.E. Georgoff, V.C. Nikolian, I. Halaweish, K. Chtraklin, P.J. Bruhn, H. Eidy, M. Rasmussen, Y. Li, A. Srinivasan, H.B. Alam, Resuscitation with Lyophilized Plasma is Safe and Improves Neurologic Recovery in a Long-Term Survival Model of Swine Subjected to Traumatic Brain Injury, Hemorrhagic Shock, and Polytrauma, Journal of Neurotrauma (2017) neu.2016.4859.

[2] O. Eroglu, T. Deniz, Ü. Kisa, P. Atasoy, K. Aydınuraz, Effect of hypothermia on apoptosis in traumatic brain injury and hemorrhagic shock model, Injury-international Journal of the Care of the Injured 48(12) (2017) S0020138317306472.

[3] M. Ito, T. Shichita, M. Okada, R. Komine, Y. Noguchi, A. Yoshimura, R. Morita, Bruton's tyrosine kinase is essential for NLRP3 inflammasome activation and contributes to ischaemic brain injury, Nature Communications 6(1) (2015) 7360-7360.

[4] H. Wu, T. Huang, L. Ying, C. Han, D. Li, Y. Xu, M. Zhang, S. Mou, Z. Dong, MiR-155 is Involved in Renal Ischemia-Reperfusion Injury via Direct Targeting of FoxO3a and Regulating Renal Tubular Cell Pyroptosis, Cellular Physiology and Biochemistry 40(6) (2016) 1692-1705.

[5] E. Sekerdag, I. Solaroglu, Y. Gursoyozdemir, Cell Death Mechanisms in Stroke and Novel Molecular and Cellular Treatment Options, Current Neuropharmacology 16 (2018) 1-1.

[6] J. Yang, F. Yao, J. Zhang, Z. Ji, K. Li, J. Zhan, Y. Tong, L. Lin, Y. He, Ischemia-reperfusion induces renal tubule pyroptosis via the CHOP-caspase-11 pathway, American Journal of Physiology-renal Physiology 306(1) (2014).

[7] P. Xia, Y. Pan, F. Zhang, N. Wang, E. Wang, Q. Guo, Z. Ye, Pioglitazone Confers Neuroprotection Against Ischemia-Induced Pyroptosis due to its Inhibitory Effects on HMGB-1/RAGE and Rac1/ROS Pathway by Activating PPAR-ɤ, Cellular Physiology and Biochemistry (2018) 2351-2368.

[8] Y. Joe, S. Kim, Y. Chen, J.W. Yang, J. Lee, G.J. Cho, J.W. Park, H.T. Chung, Tristetraprolin Mediates Anti-Inflammatory Effects of Carbon Monoxide on Lipopolysaccharide-Induced Acute Lung Injury, American Journal of Pathology 185(11) (2015) 2867-2874.

[9] N. Fujisaki, K. Kohama, T. Nishimura, H. Yamashita, M. Ishikawa, A. Kanematsu, T. Yamada, S. Lee, T. Yumoto, K. Tsukahara, Donor pretreatment with carbon monoxide prevents ischemia/reperfusion injury following heart transplantation in rats, Medical gas research 6(3) (2016) 122-129.

[10] Y. Cheng, J. Rong, Therapeutic Potential of Heme Oxygenase-1/carbon Monoxide System Against Ischemia-Reperfusion Injury, Current Pharmaceutical Design 23(26) (2017) 3884-3898.

[11] E.Y. Choi, S.H. Choe, J.Y. Hyeon, J.I. Choi, I.S. Choi, S.J. Kim, Carbon monoxide-releasing molecule-3 suppresses Prevotella intermedia lipopolysaccharide-induced production of nitric oxide and interleukin-1β in murine macrophages, European Journal of Pharmacology 764 (2015) 22-29.

[12] S. Nils, C.C. Rom?O, B. Julia, W.A. Lagrèze, L.E. Otterbein, B. Hartmut, L. Torsten, G. Ulrich, Carbon monoxide abrogates ischemic insult to neuronal cells via the soluble guanylate cyclase-cGMP pathway, Plos One 8(4) (2013) e60672.

[13] B. Egemnazarov, A. Sydykov, R.T. Schermuly, N. Weissmann, J. Stasch, A.S. Sarybaev, W. Seeger, F. Grimminger, H.A. Ghofrani, Novel soluble guanylyl cyclase stimulator BAY 41-2272 attenuates ischemia-reperfusion-induced lung injury, American Journal of Physiology-lung Cellular and Molecular Physiology 296(3) (2009).

[14] N.M. Sanna, D.J. Antoine, L.C. Peter, J.G. Lock, A.F. Nita, H.G. Kari, G. Alf, E.H. Helena, A. Ulf, S.E. Applequist, TLR activation regulates damage-associated molecular pattern isoforms released during pyroptosis, Embo Journal 32(1) (2014) 86-99.

[15] Y. Lu, S. Xu, H. Chen, M. He, Y. Deng, Z. Cao, H. Pi, C. Chen, M. Li, Q. Ma, CdSe/ZnS quantum dots induce hepatocyte pyroptosis and liver inflammation via NLRP3 inflammasome activation, Biomaterials 90 (2016) 27-39.

[16] N. Henninger, A. Heimann, O. Kempski, Electrophysiology and neuronal integrity following systemic arterial hypotension in a rat model of unilateral carotid artery occlusion, Brain Research 1163 (2007) 119-129.

[17] L. Franchi, T. Eigenbrod, R. Munozplanillo, G. Nunez, The inflammasome: a caspase-1-activation platform that regulates immune responses and disease pathogenesis, Nature Immunology 10(3) (2009) 241-247.

[18] Y. Kudo, H. Ohtaki, K. Dohi, L. Yin, T. Nakamachi, S. Endo, S. Yofu, Y. Hiraizumi, H. Miyaoka, S. Shioda, Neuronal damage in rat brain and spinal cord after cardiac arrest and massive hemorrhagic shock, Critical Care Medicine 34(11) (2006) 2820.

[19] Zhang LM, Z. DX, The Dual Neuroprotective-Neurotoxic Effects of Sevoflurane After Hemorrhagic Shock Injury, J Surg Res 235 (2019) 591-599.

[20] K.K. Ida, K.I. Chisholm, L.M.S. Malbouisson, D.B. Papkovsky, A. Dyson, M. Singer, M.R.

Duchen, K.J. Smith, Protection of cerebral microcirculation, mitochondrial function, and electrocortical activity by small-volume resuscitation with terlipressin in a rat model of haemorrhagic shock, BJA: British Journal of Anaesthesia 120(6) (2017) 1245-1254.

[21] C.S. Budinich, L.B. Tucker, D. Lowe, J. Rosenberger, J.T. Mccabe, Short and long-term motor and behavioral effects of diazoxide and dimethyl sulfoxide administration in the mouse after traumatic brain injury, Pharmacology, Biochemistry and Behavior 108 (2013) 66-73.

[22] S.W. Scheff, S.A. Baldwin, R.W. Brown, P.J. Kraemer, Morris water maze deficits in rats following traumatic brain injury: lateral controlled cortical impact, Journal of Neurotrauma 14(9) (1997) 615-627.

[23] U. Dirnagl, C. Iadecola, M.A. Moskowitz, Pathobiology of ischaemic stroke: an integrated view, Trends in Neurosciences 22(9) (1999) 391-397.

[24] H.M. Lee, D.H. Lee, J.H. Choi, S.R. Lee, Y.W. Kim, D.L. Jee, H.S. Do, H.M. Lee, S.J. Park, Sevoflurane-induced post-conditioning has no beneficial effects on neuroprotection after incomplete cerebral ischemia in rats, Acta Anaesthesiologica Scandinavica 54(3) (2010) 328.

[25] X. Hu, J. Wang, Q. Zhang, X. Duan, Z. Chen, Y. Zhang, Postconditioning with sevoflurane ameliorates spatial learning and memory deficit after hemorrhage shock and resuscitation in rats, Journal of Surgical Research 206(2) (2016) 307.

[26] S. Zhu, Z. Zhang, L. Jia, K. Zhan, L. Wang, N. Song, Y. Liu, Y. Cheng, Y. Yang, L. Guan, Valproic acid attenuates global cerebral ischemia/reperfusion injury in gerbils via anti-pyroptosis pathways, Neurochemistry International 124 (2019) 141-151.

[27] G. Zheng, Y. Zhan, H. Wang, Z. Luo, F. Zheng, Y. Zhou, Y. Wu, S. Wang, Y. Wu, G. Xiang, Carbon monoxide releasing molecule-3 alleviates neuron death after spinal cord injury via inflammasome regulation, EBioMedicine   (2019).

[28] K. Inoue, T. Takahashi, K. Uehara, H. Shimuzu, K. Ido, H. Morimatsu, E. Omori, H. Katayama, R. Akagi, K. Morita, Protective role of heme oxygenase 1 in the intestinal tissue injury in hemorrhagic shock in rats, Shock 29(2) (2008) 252-261.

[29] S.W. Ryter, A.M.K. Choi, Targeting heme oxygenase-1 and carbon monoxide for therapeutic modulation of inflammation, Translational Research the Journal of Laboratory & Clinical Medicine 167(1) (2016) 7.

[30] Y. Ryu, S. Yutaka, H. Kohji, S. Koji, O. Kotaro, NO/cGMP/PKG signaling pathway induces

magnesium release mediated by mitoKATP channel opening in rat hippocampal neurons, Febs Letters 587(16) (2013) 2643-2648.

[31] Y. He, J. Xi, H. Zheng, Astragaloside IV inhibits oxidative stress-induced mitochondrial permeability transition pore opening by inactivating GSK-3β via nitric oxide in H9c2 cardiac cells, Oxidative Medicine and Cellular Longevity,2012,(2012-9-18) 2012(9) (2012) 935738.

[32] T. Misawa, M. Takahama, T. Kozaki, H. Lee, J. Zou, T. Saitoh, S. Akira, Microtubule-driven spatial arrangement of mitochondria promotes activation of the NLRP3 inflammasome, Nature Immunology 14(5) (2013) 454-460.

[33] Y. Han, X. Xu, C. Tang, P. Gao, X. Chen, X. Xiong, M. Yang, S. Yang, X. Zhu, S. Yuan, Reactive oxygen species promote tubular injury in diabetic nephropathy: The role of the mitochondrial ros-txnip-nlrp3 biological axis, Redox biology 16 (2018) 32-46.

[34] H.B. Suliman, C.A. Piantadosi, Mitochondrial Quality Control as a Therapeutic Target, Pharmacological Reviews 68(1) (2015) 20-48.

[35] X.Y. Zhou, F. Zhang, C.J. Ying, J. Chen, L. Chen, J. Dong, Y. Shi, M. Tang, X.T. Hu, Z.H. Pan, Inhibition of iNOS alleviates cognitive deficits and depression in diabetic mice through downregulating the NO/sGC/cGMP/PKG signal pathway, Behavioural Brain Research 322 (2017) 70-82.

[36] S. Feng, D. Fox, S.M. Man, Mechanisms of Gasdermin Family Members in Inflammasome Signaling and Cell Death, Journal of Molecular Biology 430(18) (2018) 3068-3080.

[37] Y.K. Choi, T. Maki, E.T. Mandeville, S. Koh, K. Hayakawa, K. Arai, Y. Kim, M.J. Whalen, C. Xing, X. Wang, Dual effects of carbon monoxide on pericytes and neurogenesis in traumatic brain injury, Nature Medicine 22(11) (2016) 1335-1341.

[38] S. Ampawong, D. Isarangkul, P. Aramwit, Sericin ameliorated dysmorphic mitochondria in high-cholesterol diet/streptozotocin rat by antioxidative property, Experimental Biology & Medicine 242(4) (2017) 411-421.

[39] N. Mariappan, R.N. Soorappan, M. Haque, S. Sriramula, J. Francis, TNF-α-induced mitochondrial oxidative stress and cardiac dysfunction: restoration by superoxide dismutase mimetic Tempol, American Journal of Physiology-heart and Circulatory Physiology 293(5) (2007).

[40] J. Wu, L. Yang, P. Xie, J. Yu, T. Yu, H. Wang, Y. Maimaitili, J. Wang, H. Ma, Y. Yang, Cobalt Chloride Upregulates Impaired HIF-1α Expression to Restore Sevoflurane Post-conditioning-Dependent Myocardial Protection in Diabetic Rats, Frontiers in Physiology 8 (2017).

[41] D.X. Zhang, L.M. Zhang, X.C. Zhao, W. Sun, Neuroprotective effects of erythropoietin against sevoflurane-induced neuronal apoptosis in primary rat cortical neurons involving the EPOR-Erk1/2-Nrf2/Bach1 signal pathway, Biomedicine & Pharmacotherapy 87 (2017) 332.

[42] J.M. Fine, A.C. Forsberg, B.M. Stroebel, K.A. Faltesek, D.R. Verden, K.A. Hamel, E.B. Raney, J.M. Crow, L.R. Haase, K.E. Knutzen, Intranasal deferoxamine affects memory loss, oxidation, and the insulin pathway in the streptozotocin rat model of Alzheimer's disease, Journal of the Neurological Sciences 380 (2017) 164.

Figure legends

Fig. 1. Changes in somatosensory evoked potentials. (A) Representative median nerve somatosensory evoked potentials at different times during HSR. N10.3 was chosen for further serial investigations of its amplitude. (B) Changes in the amplitude of the somatosensory cortical evoked potential in response to hemorrhagic shock. Data are presented as mean ± SD (n = 6 per group). *$P < 0.05$ vs. baseline, [#]$P < 0.05$ vs. 15 min after bleeding, [&]$P < 0.05$ vs. 30 min after bleeding.

Fig. 2. Changes in cortical pyroptosis after hemorrhagic shock and resuscitation (HSR) exposure. (A) Representative photomicrographs from cleaved caspase-1/NeuN/DAPI staining (cleaved caspase-1, red; NeuN, green; DAPI, blue) showing pyroptotic cells in the cortical tissue 6–24 h after HSR. (B) Percentages of pyroptotic cells in the cortical tissue 6–24 h after HSR, scale bar = 50 μm. Data are presented as mean ± SD (n = 6 per group). *$P < 0.05$ vs. Sham, **$P < 0.05$.

Fig. 3. Experimental protocol and changes in carbon monoxide concentration caused by the indicated stimuli. (A) Sham: rats without hemorrhagic shock and resuscitation (HSR) or CORM-3 treatment; HSR: rats bled to 30 mmHg for 1 h and resuscitated by blood re-infusion for 15 min; CORM-3 or iCORM-3: after resuscitation, rats injected with CORM-3 (4 mg/kg) or iCORM-3 (4 mg/kg) as a control via the left femoral vein; and NS2028 or Vehicle: rats injected with NS2028 (10 mg/kg) or saline as a control via the left femoral vein before bleeding. (B) Carbon monoxide concentration 6–24 h after HSR. Data are presented as mean ± SD (n = 6 per group). *$P < 0.05$ vs. Sham; [#]$P < 0.05$ vs. the previous time point; for the same point, [$]$P < 0.05$ vs. HSR and HSR/iCORM-3.

Fig. 4. Changes in cortical pyroptosis, sGC activity, and cGMP content caused by the indicated stimuli. (A) Representative photomicrographs from cleaved caspase-1/NeuN/DAPI staining (cleaved caspase-1, red; NeuN, green; DAPI, blue) showing pyroptotic cells in the cortical tissue by the indicated stimuli, scale bar = 50 μm. (B) Percentages of pyroptotic cells in the cortical tissue caused by the indicated stimuli. (C) Representative Western blot of IL-1β and IL-18 in the cortical tissue. (D, E) Ratio between optical density value of IL-1β and IL-18 in the cortical tissue evaluated by Western blotting. Data are presented as mean ± SD (n = 6 per group). (F, G) Changes in the soluble guanylate-cyclase (sGC) enzyme activity and cyclic guanosine monophosphate (cGMP) content in rat cortical tissue homogenate caused by the indicated stimuli. Sham, HSR, CORM-3, iCORM-3, NS2028 and Vehicle are as described previously. *$P<0.05$ vs. Sham/iCORM/Vehicle group; †$P<0.05$ vs. the equivalent sham group; #$P<0.05$ vs. the equivalent vehicle group; $$P<0.05$ vs. the equivalent iCORM group.

Fig. 5. Changes in mitochondrial regulation of the cortical tissue caused by the indicated stimuli. (A) Dysmorphic mitochondria under an electron microscope from cortical extraction caused by the indicated stimuli, scale bar = 200 nm. (B) Percentages of normal mitochondria in the cortical tissue caused by the indicated stimuli. (C) Percentages of swelling plus ghost mitochondria in the cortical tissue caused by the indicated stimuli. (D) Changes in the mitochondrial membrane potential (MMP) of the cortical tissue caused by the indicated stimuli. (E) Changes in mitochondrial ROS of the cortical tissue caused by the indicated stimuli. Data are presented as mean ± SD (n = 6 per group). Sham, HSR, CORM-3, iCORM-3, NS2028 and Vehicle are as described previously. *$P<0.05$ vs. Sham/iCORM/Vehicle group; †$P<0.05$ vs. the equivalent sham group; #$P<0.05$ vs. the equivalent vehicle group; $$P<0.05$ vs. the equivalent iCORM group.

Fig. 6. Changes in T2-weighted MRI caused by the indicated stimuli. (A) T2-weighted MRI coronal views from rats at 24 h after HSR. (B) The ratio of standardized signal intensity on regions of cerebral cortex before/after indicated stimuli. Data are presented as mean ± SD (n = 12 per group). Sham, HSR, CORM-3, iCORM-3, NS2028 and Vehicle are as described previously. *$P<0.05$ vs. Sham/iCORM/Vehicle group; †$P<0.05$ vs. the equivalent sham group; #$P<0.05$ vs. the equivalent vehicle group; $$P<0.05$ vs. the equivalent iCORM group.

Fig. 7. Changes in learning ability caused by the indicated stimuli. (A) Computer printouts of swimming trajectories of each group on day 30 after HSR. The circle represents the platform location. (B–E) Escape latency in Morris water maze from Day 1 to Day 4. (F, G) The ratio of time and distance spent in the targeted quadrant when the platform was taken away. Data are presented as mean $\pm$ SD (n = 6 per group). Sham, HSR, CORM-3, iCORM-3, NS2028 and Vehicle are as described previously. *P<0.05 vs. Sham/iCORM/Vehicle group; †P<0.05 vs. the equivalent sham group; #P<0.05 vs. the equivalent vehicle group; $P<0.05 vs. the equivalent iCORM group.

Graphical abstract. A proposed diagram tying together the observations involved in CORM-3-induced neuroprotection against HSR. HSR increased neuronal pyroptosis, which might be associated with up-regulation of ROS. CORM-3 not only significantly reduced these neuronal pyroptosis, but also improved long-term learning ability and T2-weighted MRI, which might be associated with inhibition of mitochondrial dysfunction through regulating activity in sGC-cGMP signal pathway, whereas NS2028, a blocker of sGC, could partially inhibit these neuroprotective effects.

A

Baseline

Before bleeding

15min after bleeding

30 min after bleeding

15 min after resuscitation

B
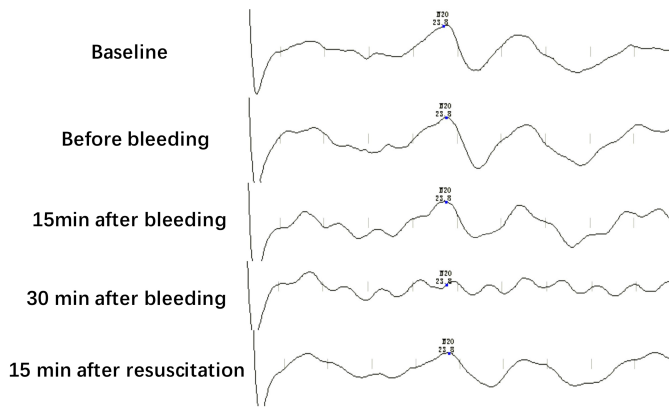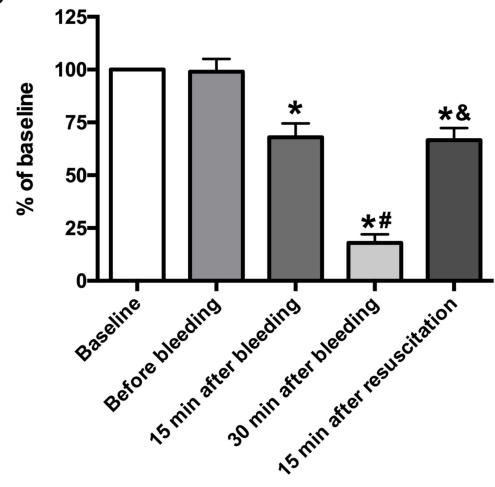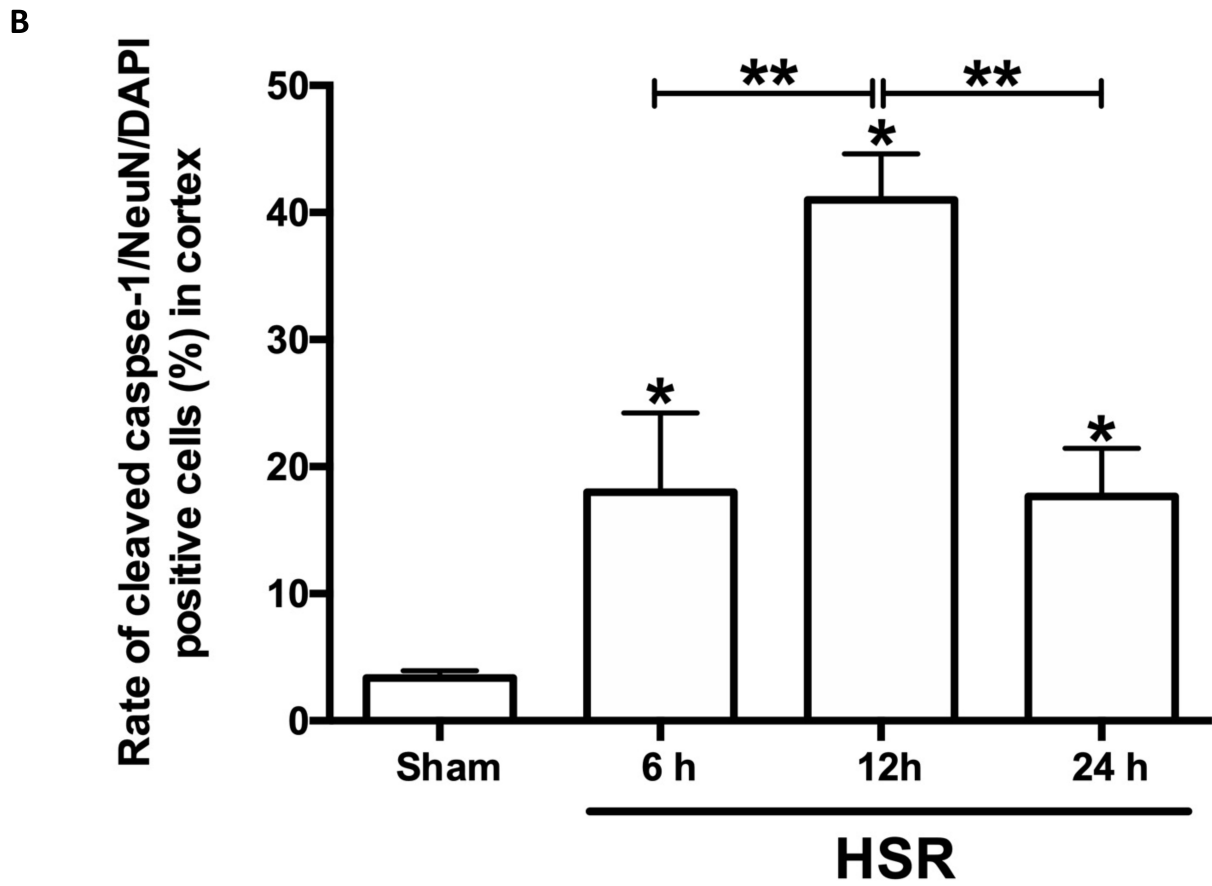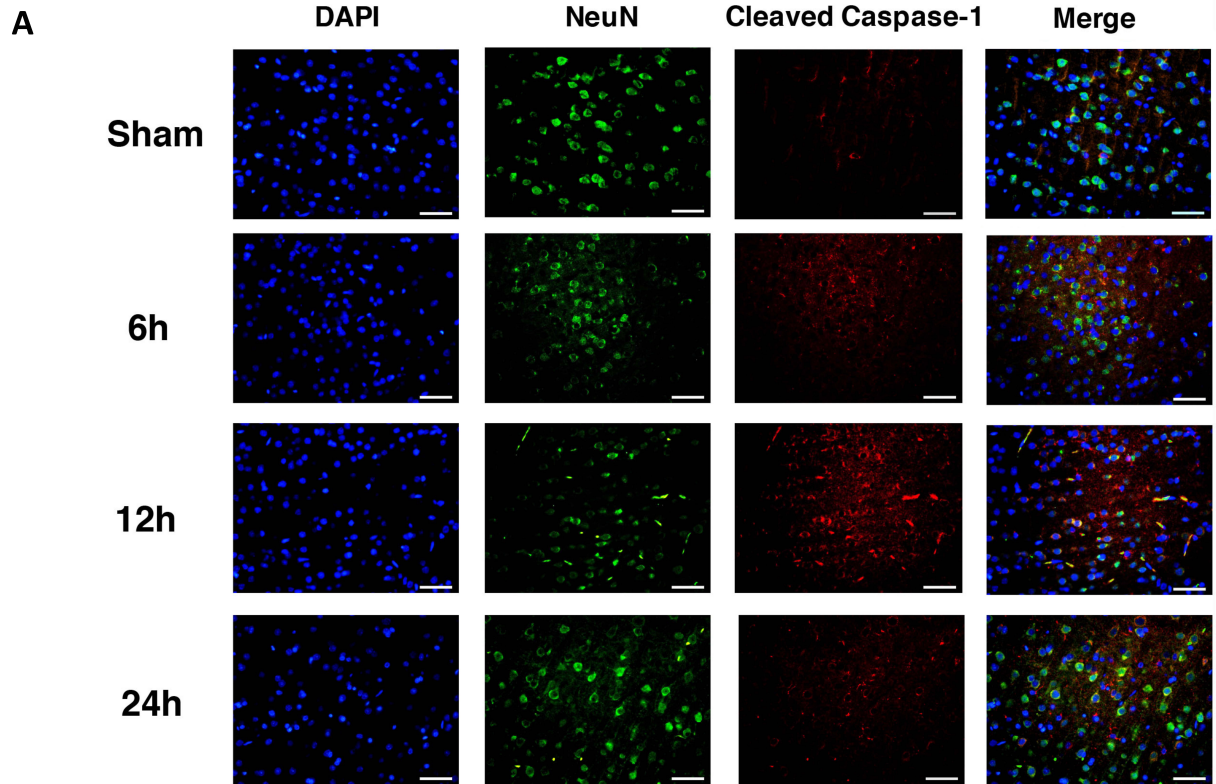
A

1: Sham/iCORM-3/Vehicle	Surgical preparation	Saline i.v.				iCORM-3 i.v.	
2: Sham/iCORM-3/NS2028	Surgical preparation	NS2028 i.v.				iCORM-3 i.v.	
3: Sham/CORM-3/Vehicle	Surgical preparation	Saline i.v.				CORM-3 i.v.	
4: Sham/CORM-3/NS2028	Surgical preparation	NS2028 i.v.				CORM-3 i.v.	
5: HSR/iCORM-3/Vehicle	Surgical preparation	Saline i.v.	Bleeding to 30 mmHg	Maintain 30 mmHg	Resuscitation to baseline	iCORM-3 i.v.	
6: HSR/iCORM-3/NS2028	Surgical preparation	NS2028 i.v.	Bleeding to 30 mmHg	Maintain 30 mmHg	Resuscitation to baseline	iCORM-3 i.v.	
7: HSR/CORM-3/Vehicle	Surgical preparation	Saline i.v.	Bleeding to 30 mmHg	Maintain 30 mmHg	Resuscitation to baseline	CORM-3 i.v.	
8: HSR/CORM-3/NS2028	Surgical preparation	NS2028 i.v.	Bleeding to 30 mmHg	Maintain 30 mmHg	Resuscitation to baseline	CORM-3 i.v.	
	20 min	1 min	15 min	45 min	15min	1 min	

B
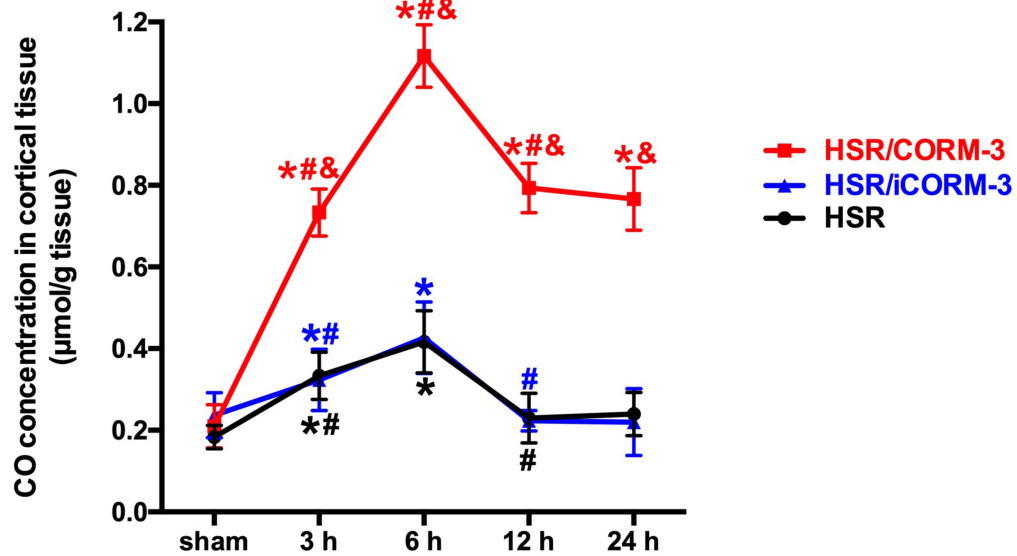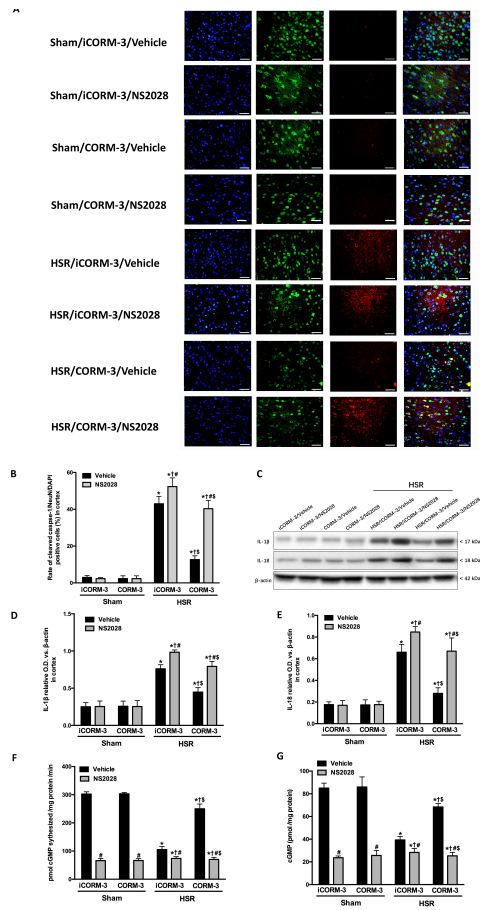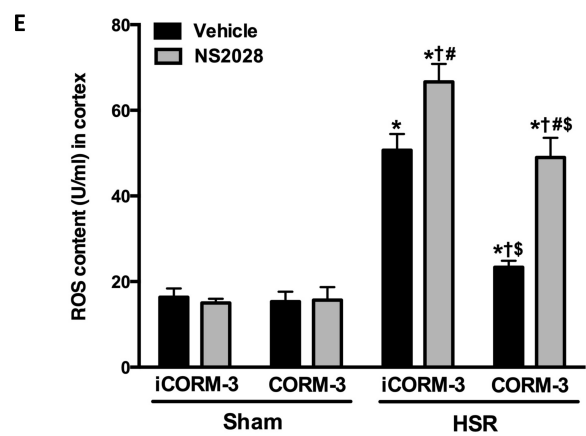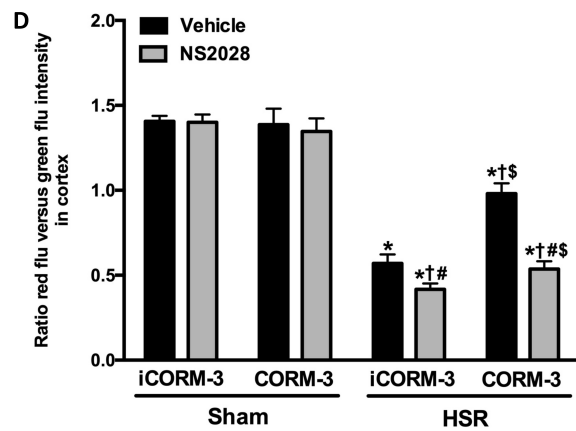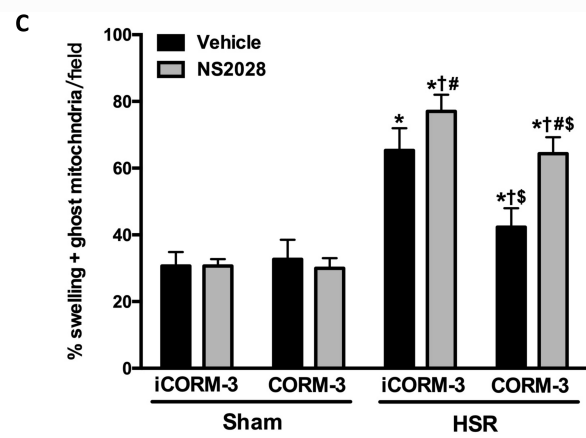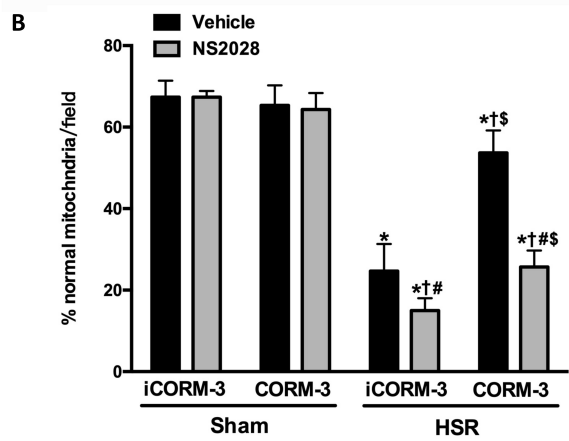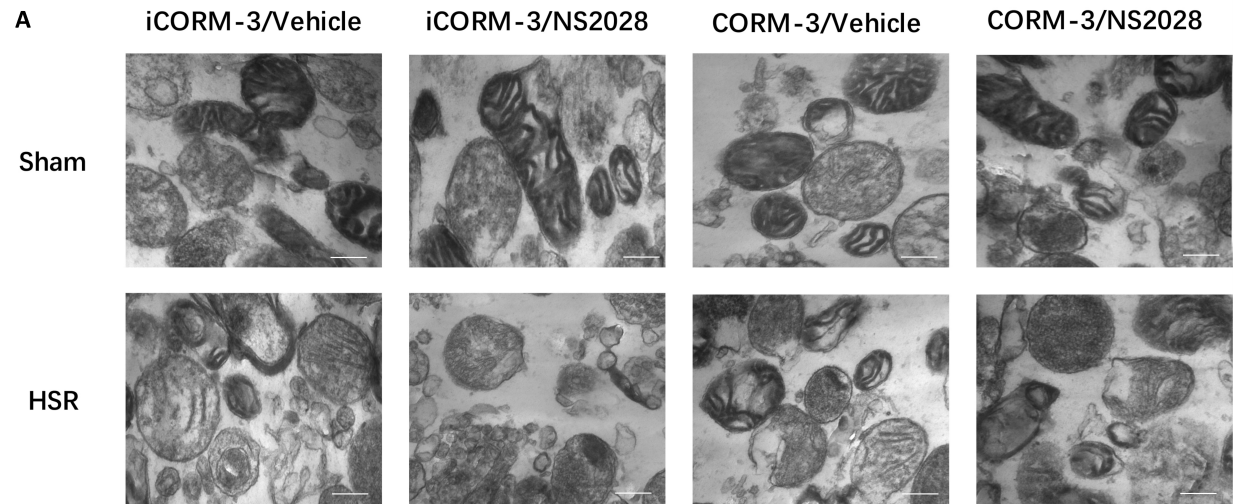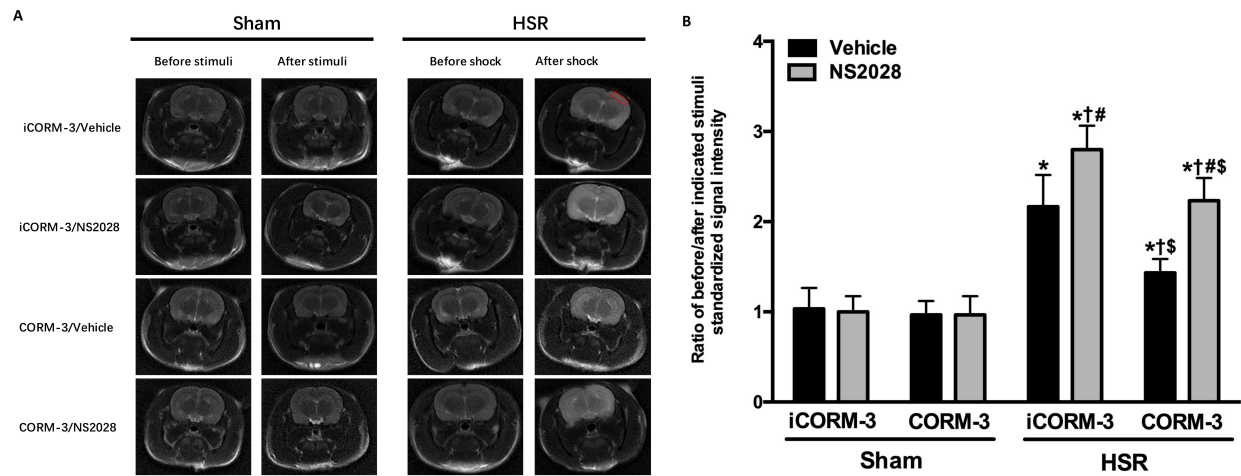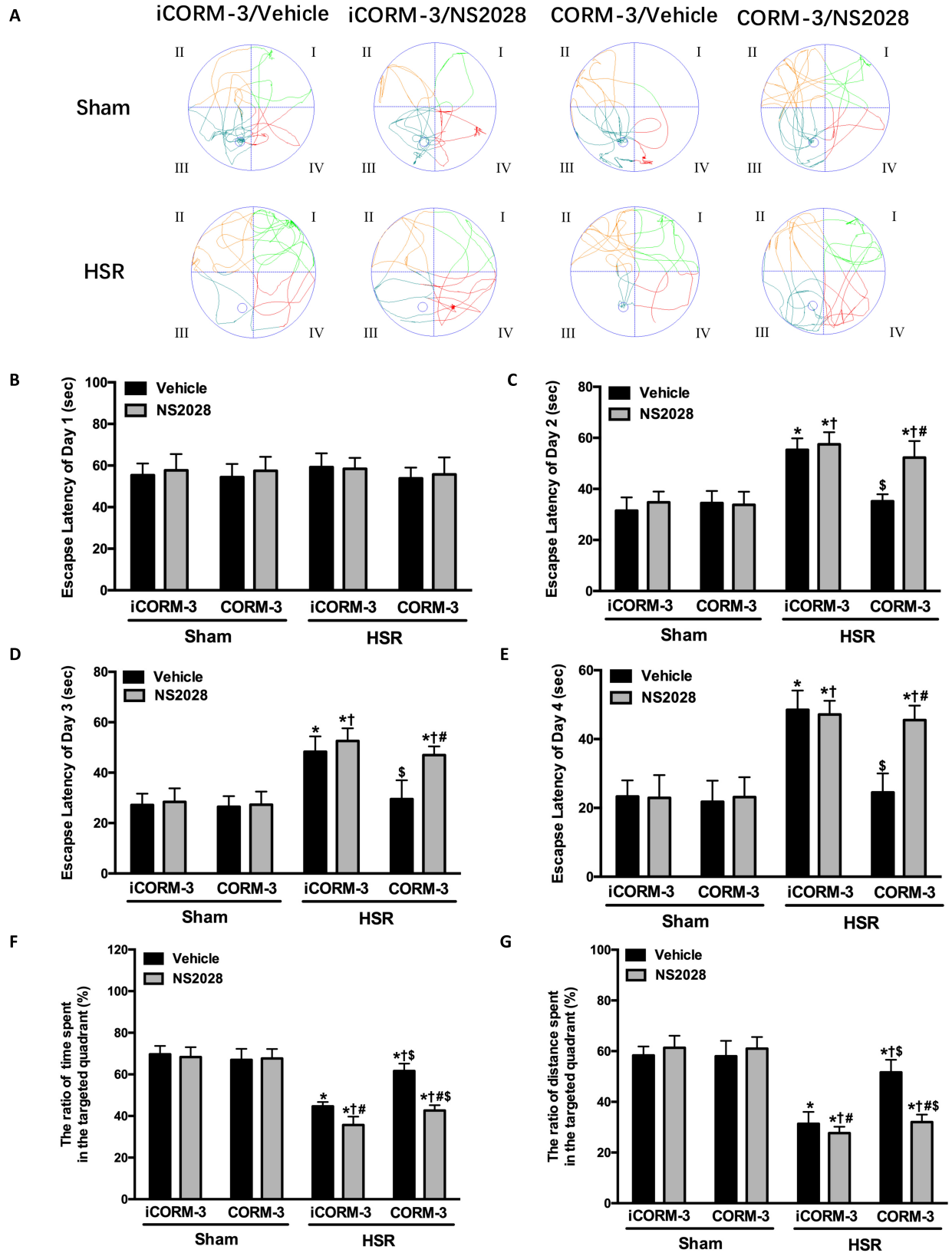
Highlights

1. Hemorrhage shock and resuscitation (HSR) significantly decreased somatosensory evoked potentials, caused degeneration of learning ability, increased cortical neuronal pyroptosis and mitochondrial injury.

2. CORM-3 administration after resuscitation provided neuroprotection for HSR, and improved learning ability.

3. The neuroprotective mechanism of CROM-3 against HSR injury could be associated with sGC–cGMP pathway.